EVIDENT

The Impact of Lithium-Ion Batteries on Renewable Energy

From Prototype to Commercial Success

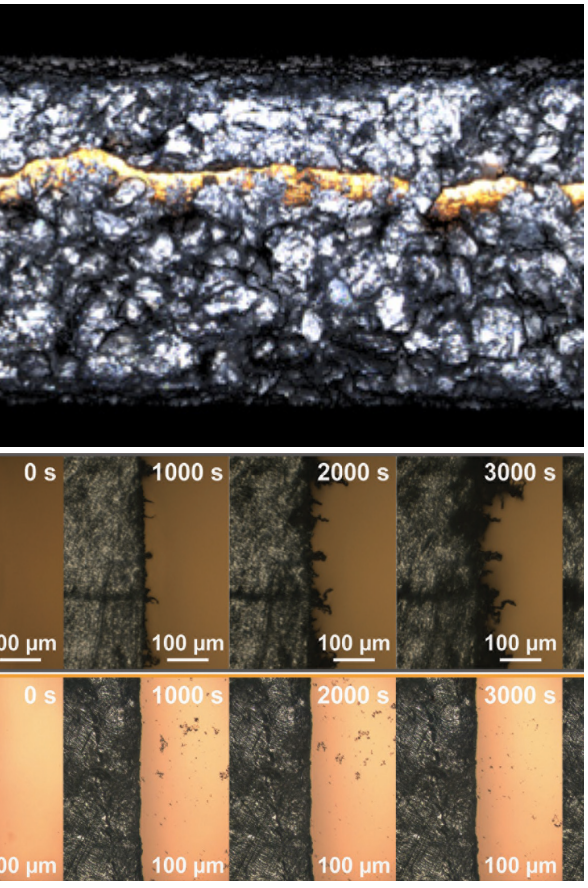

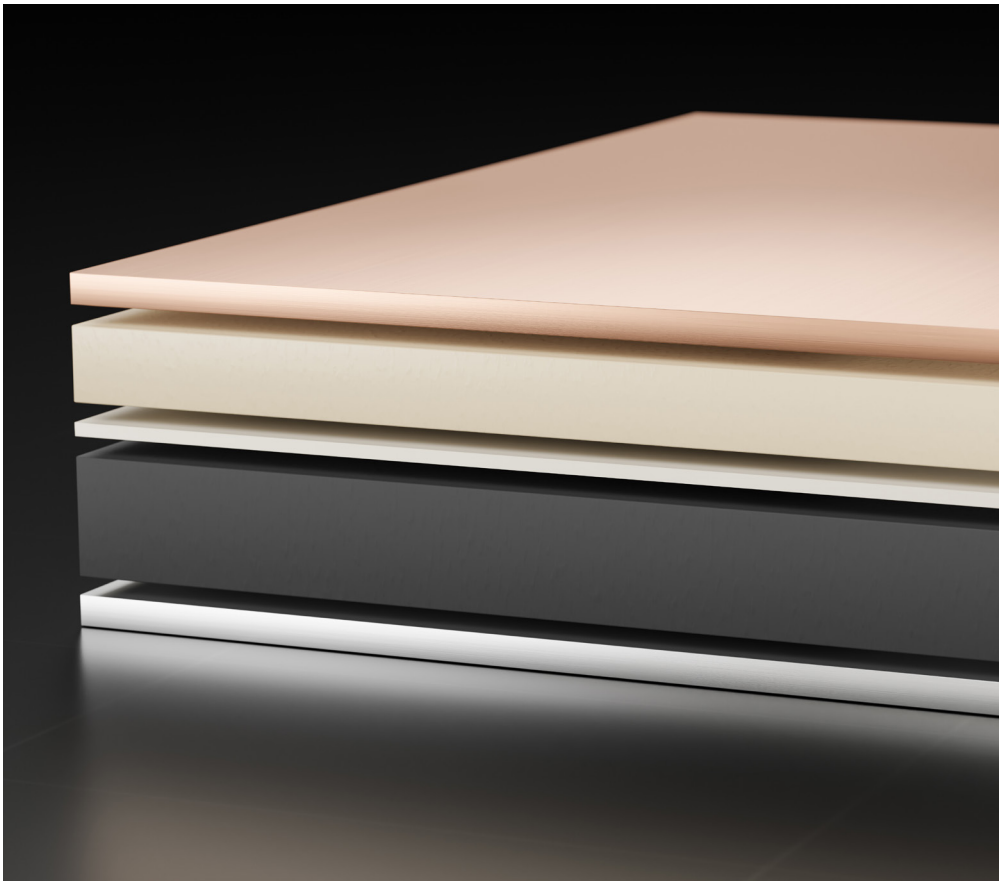

OLYMPUS

WILEY

Contents

Imprint

© Wiley-VCH GmbH
Boschstr. 12,
69469 Weinheim, Germany
Email: info@wiley-vch.de
Editors:
Dr. Cecilia Kruszynski &
Róisín Murtagh

The Evolution of Lithium-Ion Batteries and their Impact on the Renewable Energy Boom: From Prototype to Commercial Success

The fight against climate change is one of the greatest global challenges of the 21st century. In recent years, the boom in the use of non-conventional renewable energies has been accompanied by an increased interest in lithium, as lithium-based batteries provide an effective solution to the challenge of storing energy generated by intermittent sources.

Lithium is a highly reactive metal with a tendency to shed its external electron. Added to the fact that it is the lightest solid element in the periodic table, this characteristic means that it can store a large amount of energy with low weight. These characteristics make lithium a highly valuable material for battery applications.

By 2050, global demand for lithium is expected to increase by more than 950%, driven mainly by a 13-fold increase in battery-based energy storage [1]. In this context, the future of decarbonization depends, among other factors, on adequate energy storage, whether on a small scale in, for example, an electric car, or on a large scale in the distribution network. This is where lithium-ion batteries, the most competitive type of batteries at present, come into play.

A lithium-ion battery or Li-Ion battery is a type of rechargeable battery that uses lithium compounds as one of the electrodes. In 1985, Akira Yoshino developed the prototype based on earlier research by John Goodenough and other experts during the 1970s. Subsequently, a team at Sony developed the first commercial lithium-ion battery in 1991 [2]. Over the years, further advances were incorporated, especially in the use of nickel-manganese-cobalt oxide (NMC) cathodes, which improved charge density, performance, and safety.

HOW LI-ION BATTERIES WORK

In its basic functionality, a battery consists of a negative electrode (anode) and a positive electrode (cathode), separated by a conductive substance called an electrolyte. When a lithium battery is charged, it means that the lithium has shed its outer electron and is positively charged (lithium ion, Li^+). When used, electrons flow from the anode to the cathode through an external circuit in a process called *oxidation.* Voltage is generated between the two electrodes that feed the electrical device, moving the ions through the electrolyte to the opposite pole. Finally, when connected to the mains for recharging, electrons enter the negative pole,

◀ back to content

and the ions return through the electrolyte. This process is called *reduction*.

The cathode can be considered the critical component of the battery; multiple technologies and combinations with different proportions of lithium and other minerals are available to manufacture it. This composition determines the capacity and voltage of the battery, which is why the cathode has been the focus of most research and development efforts.

The electrolyte and separator determine the safety of a battery, while the cathode and anode determine its performance. For the former, materials with high conductivity are mainly used so that the lithium ions can easily move back and forth in the battery. In the production process, salts, which act as a medium for transferring lithium ions, solvents, and additives are used in small amounts for specific purposes. When created in this way, only the ions move through the electrolyte, and no electrons are allowed to pass through. The separator functions as a physical barrier between the cathode and the anode. It prevents the direct flow of electrons and allows only ions to pass through internal microscopic holes. Synthetic resins such as polyethylene and polypropylene are usually used in their manufacture. The union of all these components makes up the cells of a battery. A battery can be composed of one or more cells connected in different ways.

ADVANTAGES AND CHALLENGES

The boom in the use of lithium-ion batteries is mainly due to their high energy density and efficiency, and long lifetime [3]. Compared with traditional nickel hydride or nickel-cadmium rechargeable battery technology, lithium-ion batteries have several advantages. Mainly, they charge in less time and take longer to discharge. Additionally, they have a higher capacity, do not experience memory effects, and retain charge well when not in use.

However, like any technology, they have certain disadvantages related to protection and costs. Li-Ion batteries must incorporate systems that prevent overloads and overheating, and they are around 40% more expensive to manufacture than nickel-cadmium.

Lithium batteries can have several problems that can cause them to underperform or become a hazard. Three common issues that lithium batteries often face, which can cause short circuits and battery explosions, are overcharging, thermal runaway, and lithium dendrite growth [4]. The overcharge process is related to the current flow injected into the cell even when the cell is at its maximum capacity. On the other hand, the concept of thermal runaway refers to the temperature increase due to improper use, and lithium dendrite growth refers to the process through which the separator is perforated, and the battery electrodes are connected.

Throughout the literature review, several mechanisms have been developed to address these problems. For example, an electrical protection circuit to avoid voltage overloads [5], or a system to avoid thermal runaway [6] and the formation of lithium dendrites [7] were proposed. Other approaches include coated separators [8,9], and electrospun membranes [10]. Additionally, some efforts have focused on improving Li anode performance in rechargeable Li-Sulfur batteries, which includes creating stable artificial interfaces [11,12], using solid-state electrolytes [13,14], and innovative designs to suppress Li polysulfide shuttle in Li-S cathodes.

The surge in non-conventional renewable energy sources has spotlighted lithium's pivotal role, especially in lithium-based batteries, as a means of storing intermittent energy. Lithium-ion batteries have emerged as a competitive solution, crucial for both small-scale applications like electric vehicles and large-scale energy distribution networks. The battery's intricate components, including the cathode, anode, and electrolyte, play a fundamental role in their functionality. Despite their advantages such as high energy density and efficiency, lithium-ion batteries face challenges like protection systems and costs. Mechanisms addressing issues such as overcharging, thermal runaway, and lithium dendrite growth have been developed, underscoring the continuous pursuit of safer and more efficient lithium battery technologies. Through innovative solutions, these batteries contribute significantly to the decarbonization drive and the global transition toward sustainable energy systems. Anticipated developments will continue enhancing Li-ion battery design and performance, further expanding their application scope.

◀ back to content

References

[1] *(2017). The Growing Role of Minerals and Metals for a Low Carbon Future. The Growing Role of Minerals and Metals for a Low Carbon Future.* DOI: 10.1596/28312.

[2] Reddy, M. V. et al. (2020). Brief History of Early Lithium-Battery Development. Materials. DOI: 10.3390/ma13081884.

[3] *Hannan, M.A. et al. (2018). State-of-the-Art and Energy Management System of Lithium-Ion Batteries in Electric Vehicle Applications: Issues and Recommendations. IEEE Access.* DOI: 10.1109/ACCESS.2018.2817655.

[4] *Wen, J. et al. (2012). A Review on Lithium-Ion Batteries Safety Issues: Existing Problems and Possible Solutions. Materials Express.* DOI: 10.1166/mex.2012.1075.

[5] *Michael et al. (2019). Design of Overcharging Protection and Passive Balancing Circuits Using Dioda for Lithium-Ion Battery Management System. 2019 16th International Conference on Quality in Research (QIR): International Symposium on Electrical and Computer Engineering.* DOI: 10.1109/QIR.2019.8898267.

[6] *M. Hartmann and J. Kelly (2018). Thermal Runaway Prevention of Li-ion Batteries by Novel Thermal Management System Mark Hartmann – CTO, Outlast Technologies LLC Joe Kelly – Senior Scientist, Outlast Technologies LLC.*

[7] *Klinsmann, M. et al. (2019). Dendritic cracking in solid electrolytes driven by lithium insertion. Journal of Power Sources.* DOI: 10.1016/j.jpowsour.2019.227226.

[8] *Tu, Z. et al. (2017). Nanoporous Hybrid Electrolytes for High-Energy Batteries Based on Reactive Metal Anodes. Advanced Energy Materials.* DOI: 10.1002/aenm.201602367.

[9] *Lei, Q.-K. et al. (2020). Towards ultra-stable lithium metal batteries: Interfacial ionic flux regulated through LiAl LDH-modified polypropylene separator. Chemical Engineering Journal.* DOI: 10.1016/j.cej.2020.125187.

[10] *Patel, A. et al. (2020). High Modulus, Thermally Stable, and Self-Extinguishing Aramid Nanofiber Separators. ACS Applied Materials & Interfaces.* DOI: 10.1021/acsami.0c03671.

[11] *Hu, A. et al. (2021). An artificial hybrid interphase for an ultrahigh-rate and practical lithium metal anode. Energy & Environmental Science.* DOI: 10.1039/D1EE00508A.

[12] *Wei, J. et al. (2020). Shielding Polysulfide Intermediates by an Organosulfur-Containing Solid Electrolyte Interphase on the Lithium Anode in Lithium–Sulfur Batteries. Advanced Materials.* DOI: 10.1002/adma.202003012.

[13] *Wan, H. et al. (2021). Bifunctional Interphase-Enabled Li 10 GeP 2 S 12 Electrolytes for Lithium–Sulfur Battery. ACS Energy Letters.* DOI: 10.1021/acsenergylett.0c02617.

[14] *Liu, Y. et al. (2021). Mechanistic Investigation of Polymer-Based All-Solid-State Lithium/Sulfur Battery. Advanced Functional Materials.* DOI: 10.1002/adfm.202104863.

back to content

01 *In Situ* Derived Mixed Ion/ Electron Conducting Layer on Top of a Functional Separator for High-Performance, Dendrite-Free Rechargeable Lithium-Metal Batteries

Adapted from Yan, M. *et al.* 2023

Rechargeable lithium-metal batteries (RLBs) face cycling and safety challenges due to reactive Li and uncontrolled dendrite growth. This study introduces an Mg_3N_2-decorated separator for Li-metal surfaces to enhance anode electrochemistry. This scalable approach promises high-energy RLBs with extended cycles and improved safety, offering new battery manufacturing possibilities.

INTRODUCTION

The lithium-metal anode, with its high theoretical capacity (3,860 mAh g^{-1}) and deeply negative potential (-3.040 V vs. standard hydrogen electrode), is touted for advancing "beyond-Li-ion" batteries, offering heightened energy storage potential for emerging applications [1,2]. However, its reactivity prompts spontaneous reactions with organic electrolytes, yielding a fragile and unstable solid electrolyte interphase (SEI). This SEI fails to shield the metal or withstand volume changes during plating/stripping [3,4]. Resultant SEI breakdown and regeneration deplete Li^+ ions and electrolyte components at the interface, constraining battery life and efficiency [5]. Moreover, uneven Li-ion and electron flow foster dendrites and pits on uneven metal surfaces, risking short circuits [6,7]. Challenges of metal surface passivation and dendrite control persist for Li-metal anodes in batteries [8–10].

Previous research introduced a mixed ion/electron conducting layer (MCL) between a polymer electrolyte and the Li anode, encouraging uniform Li deposition via charge carrier manipulation [11]. This study unveils an *in situ* MCL formed on the Li anode.

RESULTS

An Mg_3N_2-Celgard (Cel) separator was created by applying the Mg_3N_2 slurry to one side of a commercial Celgard separator. During discharge, Mg_3N_2 transformed into Mg and Li_3N. Additionally, Mg formed a Li-Mg solid solution on the Li foil [12]. A qualitative experiment confirmed the alloy reaction by tightly binding a Li foil and an Mg foil at room temperature and monitoring the interface. After aging for 10 days, a blurry interface emerged, indicating spontaneous atom diffusion and the alloying reaction. Illustrated in Fig. 1a, a Li-Mg solid

back to content

solution phase formed on the upper Li anode surface, facilitating bulk rather than surface diffusion. Moreover, the Mg atom concentration likely exhibited a gradient distribution perpendicular to the interface (Fig. 1b). Consequently, the migration ability of Li atoms, varying with the Mg atom concentration gradient, became pivotal for diffusion. Diffusion coefficients of Li ions in coin cells assembled with a lithium nickel cobalt manganese oxide cathode (NCM622) and Li-Mg solid solution anode with varying Mg content were investigated via scan rate-dependent cyclic voltammetry (CV) (Fig. 1c). The diffusion coefficients of Li-Mg solid solution cells ($1.01–1.41 \times 10^{-9}$ cm^2 s^{-1}) greatly surpass those of Li anodes (2.66×10^{-10} cm^2 s^{-1}). Furthermore, the diffusion coefficient increased with higher Mg content in Li-Mg solid solution. This gradient Mg distribution enabled ultrafast diffusion on the top surface and spatially linked diffusion within the body, promoting Li^+ plating internally rather than solely on the foil's surface.

Operando optical microscopy tracked Li deposition on the bare and Mg_3N_2-protected Li anodes, using a Li foil as the counter electrode. Cross-sectional images of the bare Li anode during plating are shown in Fig. 1d and Video S1 (Supporting Information). The anode became mossy and dark due to the nano-size effect, differentiating it from the pristine Li with a metallic luster and smooth interface. Li dendrites formed during plating. Conversely, the Li anode protected by the Mg_3N_2 layer displays uniform plating without dendrites (Fig. 1e), confirming the diffusion effect of the Li-Mg alloy layer. Furthermore, the insulating Li_3N layer that formed establishes a vital potential gradient across the MCL, necessary for driving Li^+ diffusion through the layer and subsequent transfer within via Li-Mg solid solution [13].

To assess MCL's impact on stabilizing Li anodes in full cells, we conducted electrochemical NCM|Li cell tests. Using a ≈3 μm Mg_3N_2-Cel separator layer, we achieved notable cycling performance. The Mg_3N_2-Cel separator demonstrated an initial capacity of 170 mAh g^{-1} and a reversible capacity of 129 mAh g^{-1} after 600 cycles, surpassing the Celgard separator's rapid drop from 168 mAh g^{-1} to 81 mAh g^{-1}. Differential capacity (dQ/dV) curves revealed distinct interfacial dynamics during different cycles. Voltage polarization with Celgard (62.5 mV) increased more rapidly than with Mg_3N_2-Cel (23.7 mV), indicating MCL's enhanced dynamics.

MCL improved rate performance, preserving higher reversible capacity post-cycling at varying rates. This underscores MCL's role in enhancing ionic transport for high rates, promoting stability and reversibility. Pouch cells with Mg_3N_2-Cel separators powered LEDs, displaying cycling stability and efficiency. Compatibility with NCM811 cathodes resulted in a superior 135 mAh g^{-1} capacity after 200 cycles. Our Mg_3N_2-Cel separator shows promise for diverse cathodes and commercial applications.

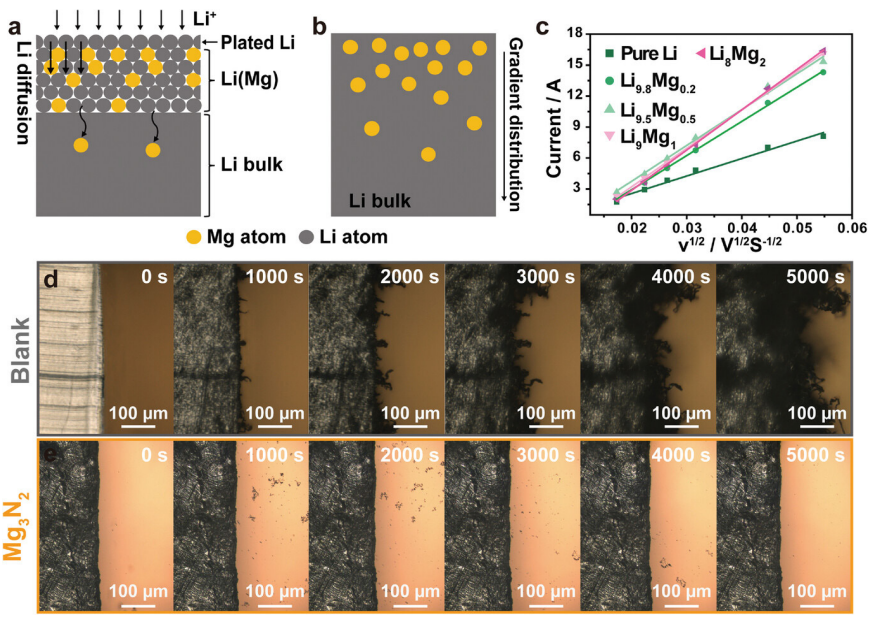

Figure 1. a) Li diffusion in Li-Mg solid solution. b) Mg gradient distribution in Li-Mg solid solution. c) Peak current vs. square root of scan rate from CV curves. *In situ* optical microscopy investigation of Li plating on d) bare Li anode and e) Mg_3N_2-treated Li anode at 4 mA cm^{-2}.

back to content

Time-of-flight secondary ion mass spectrometry (ToF-SIMS) detected even F^- distribution on the anode surface after full cell cycling, with decreased signal intensity drop during sputtering. This implies MCL reduces ionic gradient, stabilizing SEI on Li anode and boosting Li plating/stripping reversibility. In contrast, SEI without MCL exhibited strong anion aggregation post repeated cycling. Cycling without MCL increased side reaction products, underscoring the efficacy of MCL in suppressing vigorous side reactions and nurturing a stable electrolyte-Li anode interface.

CONCLUSION

An *in situ* conversion strategy stabilized the Li anode, as the resulting MCL erased ionic gradients, unified electric current, and reduced parasitic reactions on the Li anode interface. Our simple yet effective strategy using a decorated commercial separator holds potential for large-scale production and battery industrialization. This approach advances stable Li-metal anode design and hastens Li metal battery commercialization, enhancing electrochemical performance, interfacial kinetics, and safety.

EXPERIMENTAL SECTION

The coating suspension included ball-milled Mg_3N_2 powder (mass ratio 10%), polyvinylidene fluoride (PVDF) (mass ratio 1%), and N-methyl pyrrolidinone (450 rpm, 6 h). It was coated onto a commercial Celgard separator using a rod coater. After solvent evaporation (7 h, 70 °C (158 °F)), the Mg_3N_2-Cel separator was punched into 19 mm diameter circular disks.

In situ optical microscopy (OLS-4000 OLYMPUS) observed Li deposition on transparent Li symmetric cells with different separators. Real-time Li deposition was captured by removing the separators from cells with Mg_3N_2-Cel and commercial Celgard separators. ToF-SIMS (TOF.SIMS5 IONTOF GmbH) analyzed ion distribution and signal intensities with a 50 × 50 μm^2 area scanned by 20 keV Ar_n^+ (n = 1,700) beam at a 10 $\mu m\ h^{-1}$ sputter rate.

CR2032 coin cells with Li-metal anode, NCM622/NCM811 cathode, and Mg_3N_2-Cel or commercial Celgard separators were assembled. Electrolyte was 1 m $LiPF_6$ dissolved in ethylene carbonate/dimethyl carbonate/diethyl carbonate (EC/DMC/DEC, 1:1:1 by volume). Performance was evaluated between 2.8 and 4.3 V at 0.5 C with a Land CT2001A battery testing system. Critical current density was monitored by symmetric Li cells using two Li foils as electrodes and Mg_3N_2-Cel as separator. Electrochemical impedance spectroscopy (EIS) was conducted using an Autolab workstation (Metrohm) at a 10^{-1}–10^5 Hz frequency range with a 10 mV amplitude.

REFERENCES

[1] Wang, J. et al. (2019). Improving cyclability of Li metal batteries at elevated temperatures and its origin revealed by cryo-electron microscopy. Nature Energy. DOI: 10.1038/s41560-019-0413-3.

[2] Jie, Y. et al. (2020). Enabling High-Voltage Lithium Metal Batteries by Manipulating Solvation Structure in Ester Electrolyte. Angewandte Chemie. DOI: 10.1002/ange.201914250.

[3] Liu, X. et al. (2020). Novel Organophosphate-Derived Dual-Layered Interface Enabling Air-Stable and Dendrite-Free Lithium Metal Anode. Advanced Materials. DOI: 10.1002/adma.201902724.

[4] Wang, Z. et al. (2020). Toward safer solid-state lithium metal batteries: a review. Nanoscale Advances. DOI: 10.1039/D0NA00174K.

[5] Liu, T. et al. (2019). Protecting the Lithium Metal Anode for a Safe Flexible Lithium-Air Battery in Ambient Air. Angewandte Chemie. DOI: 10.1002/ange.201911229.

[6] Yan, M. et al. (2019). Interfacial design for lithium–sulfur batteries: From liquid to solid. EnergyChem. DOI: 10.1016/j.enchem.2019.100002.

[7] Lu, D. et al. (2015). Failure Mechanism for Fast-Charged Lithium Metal Batteries with Liquid Electrolytes. Advanced Energy Materials. DOI: 10.1002/aenm.201400993.

[8] Yao, X. et al. (2023). Surface Bromination of Lithium-Metal Anode for High Cyclic Efficiency. Advanced Energy Materials. DOI: 10.1002/AENM.202203233.

[9] Feng, W. et al. (2023). Enhanced Moisture Stability of Lithium-Rich Antiperovskites for Sustainable All-Solid-State Lithium Batteries. Advanced Materials. DOI: 10.1002/ADMA.202210365.

[10] Liang, J. et al. (2023). Halide Layer Cathodes for Compatible and Fast-Charged Halides-Based All-Solid-State Li Metal Batteries. Angewandte Chemie. DOI: 10.1002/ANGE.202217081.

[11] Yan, M. et al. (2020). Stabilizing Polymer–Lithium Interface in a Rechargeable Solid Battery. Advanced Functional Materials. DOI: 10.1002/adfm.201908047.

[12] Obrovac, M.N. and Chevrier, V.L. (2014). Alloy Negative Electrodes for Li-Ion Batteries. Chemical Reviews. DOI: 10.1021/cr500207g.

[13] Liang, X. et al. (2017). A facile surface chemistry route to a stabilized lithium metal anode. Nature Energy. DOI: 10.1038/nenergy.2017.119.

◀ back to content

02 Phase Separation-Controlled Assembly of Hierarchically Porous Aramid Nanofiber Films for High-speed Lithium-Metal Batteries

Adapted from Jung, A. *et al.* 2022

This study shows that hierarchically porous aramid nanofiber separators effectively inhibit lithium dendrite growth, ensuring stable high-rate cycle performances, and addressing Li-metal battery lifespan and safety.

INTRODUCTION

With their high capacity and low electrochemical reduction potential, lithium-metal anodes have accumulated interest in the realm of high-energy Li rechargeable batteries. However, they grapple with issues such as short lifespans, low efficiency, and safety concerns arising from the growth of Li dendrites [1–3]. Various approaches, including coated separators [4,5] and electrospun membranes [6], were explored to address this. We presented hierarchically porous aramid nanofibrils (PANF) separators with over 97% porosity, achieved via a two-step solvent exchange process. Such micro and nanoscale porous separators offer a promising strategy for enhanced cycling performance at high rates.

RESULTS

Fabrication of PANF Films by Two-Step Solvent Exchange Process

Aramid nanoseed dispersions resulted from aramid fibers' excess KOH protonation in dimethyl sulfoxide (DMSO). Nanoseed solutions were coated onto a glass via bar coating, followed by initial protic solvent immersion. Protonated aramid nanoseeds self-assembled into nano-fibrillar networks through solvent exchange, restoring amide group hydrogen bonds. Initial solvents included deionized (DI) water, ethanol, and isopropyl alcohol (IPA), with DI water for the second step. PANF samples with various solvents were labeled EPANF, DPANF, and IPANF for the mentioned initial solvents, respectively. Initial thicknesses of 50, 100, and 150 μm were named EPANF, EPANF100, and EPANF150, respectively. Freeze-drying preserved structural integrity.

PANF film porous structures were analyzed with field emission scanning electron microscopy (FE-SEM) (Fig. 1a–c). EPANF exhibited highly porous structures with 7.7 ± 3.9 μm diameter macropores (Fig. 1b). The inset (Fig. 1b) highlighted 17.6 ± 5.5 nm nanopores and randomly entangled ANFs of 23.3 ± 8.0 nm diameter. IPANF had the largest pores (17.7 ± 2.8 μm) but was mechanically unstable (Fig. 1c). DPANF showed a dense nano-fibrillar structure without macropores (Fig. 1a). The PANF films exhibited variations in morphology but not in chemical structure.

It was found that the first solvent exchange determined a porous structure (Fig. 1d–h). Higher pKa solvents like ethanol and IPA yielded less reprotonation (Fig. 1h), yielding films that displayed color changes (Fig. 1d–f). DI water immersion caused immediate opaque white

back to content

color due to rapid reprotonation. IPA immersion showed reddish-yellow color after 1 min, shifting to pale yellow after 30 min, indicating partial reprotonation. Ethanol immersion showed intermediate color change, aligned with UV-Vis results. Optical microscopy images (Fig. 1g) depicted gelation-induced phase separation mainly in the first step, preserved until the second step.

Higher pKa solvents like ethanol and IPA yielded less reprotonation, leading to less fibrillization, yielding less dense gel films, and higher phase separation (Fig. 1a–h). Differences in the solubility parameter of aramid nanofibers ($\delta_{aramid} \approx 23.0$ MPa$^{0.5}$) [7] and immersion solvents ($\delta_{isopropanol} \approx 21.5$, $\delta_{ethanol} \approx 26.0$, $\delta_{water} \approx 47.9$ MPa$^{0.5}$) [8] influenced phase separation rate and film porosity. Larger differences accelerated phase separation, yielding denser films. Smaller solubility differences caused gelated aramid nanofibers to swell, forming looser polymeric gel films. In the second exchange step, primary solvents were replaced with water, promoting rapid, dense nano-fibrillar network structure formation from non-reacted aramid portions, ensuring complete fibrillization.

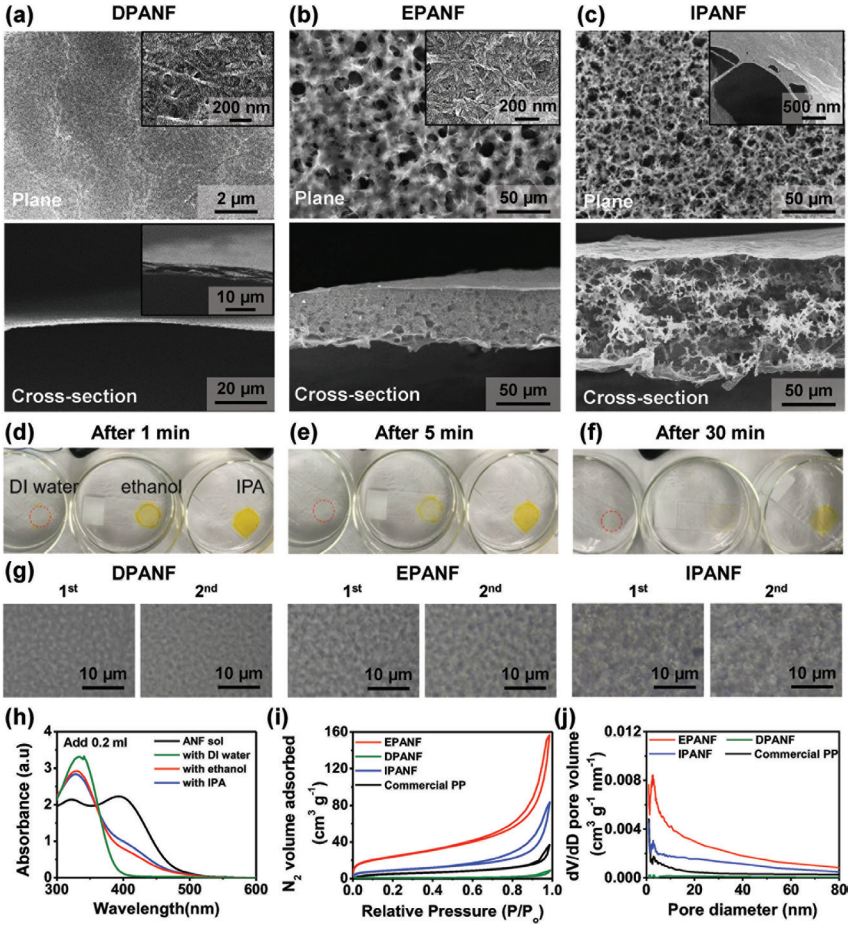

Figure 1: a) FE-SEM images of DPANF, EPANF, and IPANF, showing cross-sections and planes. Insets present magnified images for each sample. Photographs of cast aramid sol films immersed in DI water (left), ethanol (middle), and IPA (right) baths for d) 1, e) 5, and f) 30 min. DI water-treated sample rapidly turned opaque white pre-1 min. Red-dashed circles denote DI water samples. g) OM images of PANF samples at each solvent exchange step. h) UV-Vis spectra of 0.005 wt% aramid solutions after adding 0.2 mL DI water, ethanol, and IPA solvents. I) BET nitrogen adsorption-desorption isotherms and j) pore distribution data for EPANF, DPANF, IPANF, and commercial PP films.

The porosities of DPANF, EPANF, and IPANF were 54.3%, 97.2%, and 98.4%, respectively. EPANF and IPANF displayed porosities over 97%, twice that of commercial polypropylene (PP) membranes (47.6%). Measurements of surface area from gas adsorption assessed nanosized pores, with EPANF having the highest pore volume (0.228 cm^3 g^{-1}) and surface area (81.6 m^2 g^{-1}). Conversely, IPANF exhibited notable porosity yet moderate pore volume and surface area, consistent with FE-SEM images (Fig. 1c), primarily macropores. DPANF exhibited the smallest pore volume and surface area among PANF samples,resembling typical single-exchange prepared aramid membranes [6,9].

Li-Metal Battery Full Cell Test

Li iron phosphate (LFP)/Li full cell-specific capacities were evaluated via step cycles, increasing the charge rate from 1 to 30 C, and returning to 1 C within a 2.5–4.2 V voltage window. LFP loading was 2–3 mg cm^{-2}. EPANF separators exhibited higher capacity retention in most steps than commercial PP. Results underscore EPANF's high capacity retention after 1,000 cycles at high C rates, outperforming most reported separators for Li-metal batteries. Furthermore, step cycle outcomes with 9 mg cm^{-2} LFP loading exhibited higher EPANF capacity retention than commercial PP at 1 to 5 C.

CONCLUSION

A two-step solvent exchange process crafted porous aramid nanofiber separators. Controlled reprotonation achieved dual porosity at micro and nanoscales. Sequential ethanol and water exchange yielded 97% porosity with nanopores in the macroporous polymer frame due to aramid nanofiber strength. Li/Li symmetric cells using EPANF showed stable cycling capacity.

back to content

Hierarchical porous structures effectively address dendrite issues in Li-metal anodes, while rapid charge/discharge capabilities offer promise for high-power energy storage.

EXPERIMENTAL SECTION

A 1.25% aramid nanoseed solution formed by stirring Kevlar 69 (Thread Exchange) and potassium hydroxide (KOH, 90%, Sigma-Aldrich) in DMSO (99.5%, Daejung Chemicals) at 27 °C (80.6 °F) for 2 weeks. KOH dissolved in DMSO (1 g/100 mL). Next, 10 mL of the 1.25% aramid sol solution was drop-coated onto a 10 cm diameter glass plate at 300 rpm for 30 s or cast onto a 10 × 10 cm glass plate using bar coating. Coated glass plates were immediately immersed for 30 min in one of the protic solvents: DI water, ethanol (95.0%, Samchun Chemicals), or IPA (99.5%, Samchun Chemicals), as the first exchange step. The resulting samples were labeled DPANF, EPANF, and IPANF. In the second exchange step, the samples were immersed in DI water for an additional 30 min and rinsed with DI water. Gel films were placed in a liquid nitrogen cooling bath and lyophilized to yield highly porous samples. For bar-coated samples, gap heights of 200, 250, and 300 μm were used for DPANF, EPANF100, and EPANF150, respectively. Prior to electrochemical tests, samples were vacuum-dried at 120 °C (248 °F) for 12 h to eliminate residual moisture.

Li surface morphologies were examined using optical microscopy (ECLIPSE LV100ND, Olympus BX51). Electrode samples were washed with ethylene carbonate (EC)/diethyl carbonate (DEC)/ dimethyl carbonate (DMC) solution and dried at 80 °C (176 °F) for 24 h in a glovebox before imaging. After disassembly, PANF samples underwent washing with an EC/DEC/DMC solution and DI water, followed by freeze-drying. Porous characteristics were examined using nitrogen adsorption isotherm measurements, and the absorbance of aramid solutions was analyzed using UV-Vis spectrometry.

REFERENCES

[1] Sun, Y. et al. (2020). Boosting the Optimization of Lithium Metal Batteries by Molecular Dynamics Simulations: A Perspective. Advanced Energy Materials. DOI: 10.1002/aenm.202002373.

[2] Xu, W. et al. (2014). Lithium metal anodes for rechargeable batteries. Energy Environ. Sci. DOI: 10.1039/C3EE40795K.

[3] Tarascon, J.-M. and Armand, M. (2001). Issues and challenges facing rechargeable lithium batteries. Nature. DOI: 10.1038/35104644.

[4] Tu, Z. et al. (2017). Nanoporous Hybrid Electrolytes for High-Energy Batteries Based on Reactive Metal Anodes. Advanced Energy Materials. DOI: 10.1002/aenm.201602367.

[5] Lei, Q.-K. et al. (2020). Towards ultra-stable lithium metal batteries: Interfacial ionic flux regulated through LiAl LDH-modified polypropylene separator. Chemical Engineering Journal. DOI: 10.1016/j.cej.2020.125187.

[6] Patel, A. et al. (2020). High Modulus, Thermally Stable, and Self-Extinguishing Aramid Nanofiber Separators. ACS Applied Materials & Interfaces. DOI: 10.1021/acsami.0c03671.

[7] Aharoni, S.M. (1992). The solubility parameters of aromatic polyamides. Journal of Applied Polymer Science. DOI: 10.1002/app.1992.070450507.

[8] Brandrup, J. and Immergut, E.H. (1966). Polymer Handbook, Interscience Publishers.

[9] Tung, S.-O. et al. (2015). A dendrite-suppressing composite ion conductor from aramid nanofibres. Nature Communications. DOI: 10.1038/ncomms7152.

back to content

03 Direct Tracking of Additive-Regulated Evolution on the Lithium Anode in Quasi-Solid-State Lithium–Sulfur Batteries

Adapted from Liu, G.-X. *et al.* 2022

Complex issues with Li anodes impede the practical use of quasi-solid-state lithium-sulfur (QSSLS) batteries. Challenges stem from unclear interfacial processes and reaction mechanisms. This study investigates insoluble sulfide stacking and Li dendrite growth on Li anodes in operational QSSLS batteries.

INTRODUCTION

Lithium-sulfur (Li-S) batteries hold promising energy storage potential, yet face challenges like limited capacity and lifespan. Intrinsic issues include S cathode drawbacks such as poor electronic conductivity and cathode volume change [1]. Li anodes also encounter hurdles, like heterogeneous solid electrolyte interphase (SEI) formation from electrolyte decomposition [2], non-uniform Li metal deposition causing dendrite growth [3], and lithium polysulfide (LiPS) shuttle between cathode and anode during discharging/charging [4]. This leads to severe LiPS reactions and hazardous Li metal anode. These reactions, along with uneven Li deposition, deplete active materials, reduce battery capacity, and pose safety risks.

So far, initial efforts have focused on improving Li anode performance in rechargeable Li-S batteries, including creating stable artificial interfaces [5,6], using solid-state electrolytes (SSEs) [7,8], and innovating configurations to suppress LiPS shuttle [9]. Notably, adding $LiNO_3$ to the electrolyte, a traditional approach, has proven effective in enhancing battery performance [10].

This study delves into the morphological evolution and dynamic processes of the Li anode within quasi-solid-state Li-S (QSSLS) cells, utilizing gel polymer electrolyte (GPE). The investigation employs *in situ* multiscale and multispectral analyses.

RESULTS

Morphological Evolution on the Li Anode in a QSSLS Cell

In situ optical microscopy (OM) observed electrolyte changes during discharging in the GPE-based QSSLS cell with a composite S cathode as the working electrode, and Li anode as the counter electrode and reference electrode. The *in situ* OM cell setup is illustrated in Fig. 1a, b, and Fig. 1c presents the cyclic voltammetry (CV) curve of the GPE-based QSSLS cell. The electrolyte near the composite S cathode turned orange during discharging to 2.32 V (Fig. 1e), indicating LiPS dissolution into GPE. As the potential reached 2.05 V, the orange spread towards the Li anode (Fig. 1f, g), signifying the LiPS shuttle.

back to content

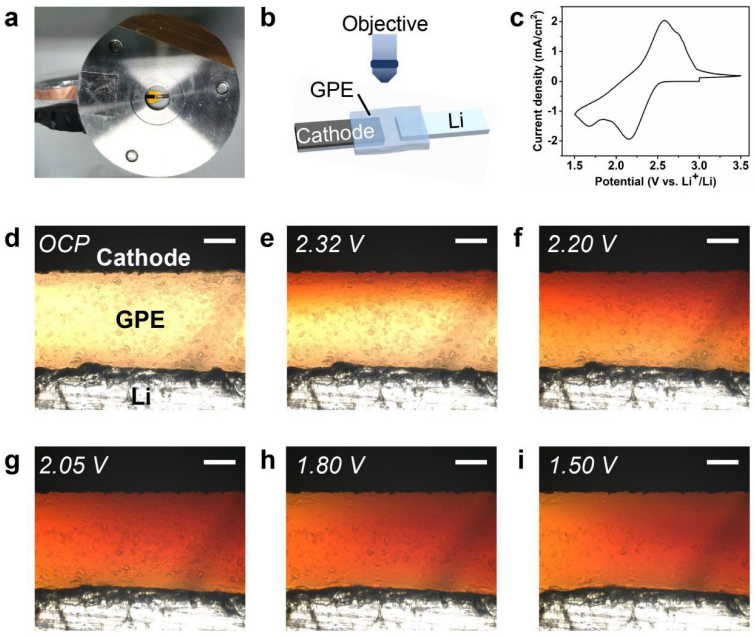

Figure 1: (a) The optical image of *in-situ* OM cell. (b) The schematic diagram of internal fabrication of *in-situ* OM cell. (c) The CV curve of the GPE-based QSSLS cell with the sweep rate of 0.5 mV/s. *In-situ* OM images of a GPE-based QSSLS cell (d) at the open circuit potential (OCP) and upon discharging to (e) 2.32 V, (f) 2.20 V, (g) 2.05 V, (h) 1.80 V and (i) 1.50 V. The scale bars are 100 μm.

Spherical particles emerged on the Li anode surface during discharging to 2.05 V, coinciding with the LiPS shuttle. Due to the Li metal anode's reactivity, these particles were likely products of LiPS and Li reactions. Reversing potential to 1.99 V caused significant deformation of the Li anode surface. Blocky deposits formed during charging from 2.35 to 2.45 V, increasing as potential neared 2.55 V, possibly from Li deposition. Rapid Li chunk growth led to elongated dendrite formation. Later, Li deposits were partially stripped during the second discharging, displaying Li deposition/dissolution irreversibility. Accumulated discharging by-products exposed significant LiPS erosion on the Li anode, and uneven Li deposition with dendrite propagation further undermined interfacial stability.

Li Anode Protection by the On-Site Formed SEI

In addressing anode degradation in the GPE-based QSSLS cell, 2 wt% $LiNO_3$ was added to the GPE (labeled 2N-GPE) to enhance interfacial behaviors. During discharging, round byproducts continued to form on the Li anode, and Li deposits displayed lumps with poor stripping reversibility. Consequently, additive content was raised to 5 wt% to optimize the Li anode in QSSLS cells (labeled 5N-GPE). Results show nanoparticles (NPs) formed at the open circuit potential (OCP) and during discharging, constituting the SEI on the Li anode in the 5N-GPE-based QSSLS cell. Furthermore, the compact SEI regulated Li deposition homogeneity, improved plating/stripping reversibility, and fostered a stable Li anode/electrolyte interface.

Cyclic Behaviors of Li Deposition

To further explore Li deposition cyclic behavior, *in situ* OM tests were conducted in QSSLS cells with different electrolytes. In the GPE-based cell, the Li anode surface is clean at OCP (Fig. 2a). Li dendrites form at Li/GPE interface and grow within GPE during initial charging (Fig. 2b). Only partial dendrite dissolution occurs during the second discharge (Fig. 3). After three cycles, more dendrites elongate toward the composite S cathode (Fig. 2c). By the tenth cycle, dendrites further extend (Fig. 2d), confirming dendrite growth and Li/GPE interface deterioration during cycling. Improved Li deposition uniformity is seen in a 2N-GPE-based cell (Fig. 4). Initial cycles exhibit uniform volume expansion of Li anode (Fig. 4b,c), with slight dendrite formation during the tenth charging (Fig. 4d). With 5 wt% $LiNO_3$ in GPE, Li deposits uniformly cover the Li anode during initial charging (Fig. 2f), remaining dendrite-free even after ten cycles (Fig. 2h). These *in situ* OM findings provide strong evidence that the cyclic performance of Li/electrolyte interface improves significantly in QSSLS batteries with 5N-GPE.

back to content

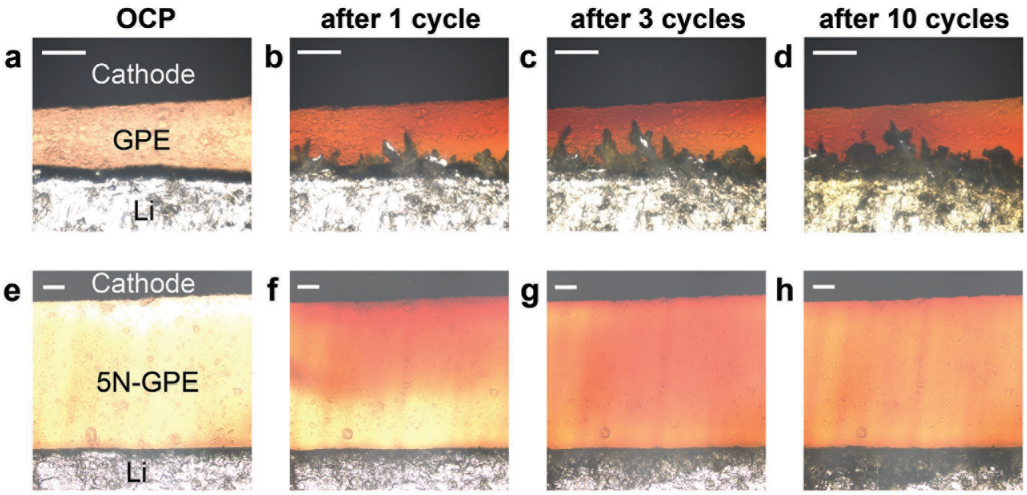

Figure 2: a) *In situ* OM imaging of the Li precipitation morphology at the Li anode/electrolyte interface at the OCP, b) after one cycle, after c) three and d) ten cycles in pristine GPE, and e) at the OCP, f) after one cycle, after g) three and h) ten cycles in 5N-GPE in QSSLS cells. The scale bars are 100 µm.

Figure 3: *In situ* OM image of the dissolving process of the Li dendrites during the second discharging in the GPE-based QSSLS cell. The scale bars are 100 µm.

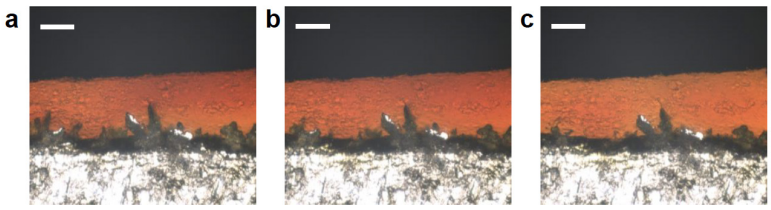

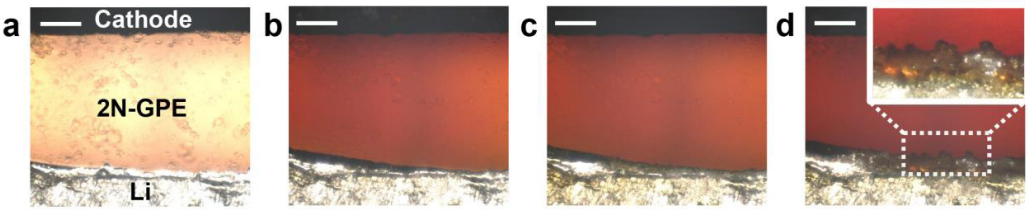

Figure 4: *In situ* OM images of the Li precipitation morphology at the Li anode/electrolyte interface at the OCP (a), after 1 cycle (b), after 3 (c) and 10 (d) cycles in 2N-GPE in QSSLS cell. The scale bars are 100 µm.

back to content

Chemical Characterization of the Li Anode Surface

Electrochemical impedance spectroscopy (EIS) tests explored QSSLS cell electrochemical performance and revealed lower interfacial impedance in 5N-GPE. 5N-GPE-based cells exhibit higher capacity and superior cycling stability compared to GPE or 2N-GPE cells. High interfacial resistance and capacity fading in GPE-based cells result from discharging products, Li dendrite growth, and Li deposition/dissolution irreversibility. $LiNO_3$-regulated SEI formation prevents LiPSs/Li side reactions and homogenizes Li deposition, enhancing cycling performance. *In situ* and *ex situ* analyses unveil varying interphase layer composition in different electrolytes, shedding light on the Li anode/electrolyte interface reaction mechanism in QSSLS cells.

CONCLUSIONS

$Li/LiNO_3$ reaction and $LiNO_3$-LiPSs synergy form a dense SEI film on Li anode, curbing active Li and LiPSs side reactions in $LiNO_3$-enhanced GPE. Uniform Li deposition and reversible deposition/dissolution enhance interface stability and cycling. These observations and additive-driven principles enhance QSSLS battery interfacial understanding, guiding optimization.

EXPERIMENTAL SECTION

Sulfur, Super P carbon, and poly(vinyl difluoride) binder (mass ratio 6:3:1) were mixed in *N*-1-methyl-2-pyrrolidone for the cathode. This mixture was coated on carbon-coated Al foil and dried at 60 °C (140 °F) for 6 h, achieving ~2.5 mg cm^{-2} active material loading. Electrolyte comprised polyethylene oxide, lithium bis (trifluoromethanesulfonyl)imide (LiTFSI), SiO_2 in tetraethylene glycol dimethyl ether (TEGDME) (TEGDME:LiTFSI = 4:1). Photoinitiator (1) and monomer (ethoxylated trimethylolpropane triacrylate; 1:100) were added, heated at 50 °C (122 °F) for 4 h, and UV-polymerized for 10 min to form GPE. GPE electrolytes with 2 and 5 wt% $LiNO_3$ were prepared.

The composite cathode and Li anode were encapsulated together, after which the GPE was polymerized *in situ* within a homemade electrochemical OM cell. The sealed cell was placed in a container with an optical window and a sealed ring. All work was conducted in an Ar-filled glovebox. *In situ* OM used an Olympus OLS4000 optical microscope with a 10X objective lens (MPlanFLN, NA 0.3). The sealed cell was connected to the electrochemical workstation for *in situ* OM. Potential was swept from OCP to 1.5 V during discharge and from OCP to 3.5 V during charge at 0.5 mV s^{-1} scan rate, referenced to Li^+/Li.

REFERENCES

[1] Van Noorden, R. (2013). Sulphur back in vogue for batteries. Nature. DOI: 10.1038/498416a.

[2] Shi, Y. et al. (2021). In-situ nanoscale insights into the evolution of solid electrolyte interphase shells: revealing interfacial degradation in lithium metal batteries. Science China Chemistry. DOI: 10.1007/s11426-020-9984-9.

[3] Shi, Y. et al. (2020). Interfacial Evolution of Lithium Dendrites and Their Solid Electrolyte Interphase Shells of Quasi-Solid-State Lithium-Metal Batteries. Angewandte Chemie International Edition. DOI: 10.1002/anie.202001117.

[4] Hou, L.-P. et al. (2021). Challenges and promises of lithium metal anode by soluble polysulfides in practical lithium–sulfur batteries. Materials Today. DOI: 10.1016/j.mattod.2020.10.021.

[5] Hu, A. et al. (2021). An artificial hybrid interphase for an ultrahigh-rate and practical lithium metal anode. Energy & Environmental Science. DOI: 10.1039/D1EE00508A.

[6] Wei, J. et al. (2020). Shielding Polysulfide Intermediates by an Organosulfur-Containing Solid Electrolyte Interphase on the Lithium Anode in Lithium–Sulfur Batteries. Advanced Materials. DOI: 10.1002/adma.202003012.

[7] Wan, H. et al. (2021). Bifunctional Interphase-Enabled Li 10 GeP 2 S 12 Electrolytes for Lithium–Sulfur Battery. ACS Energy Letters. DOI: 10.1021/acsenergylett.0c02617.

[8] Liu, Y. et al. (2021). Mechanistic Investigation of Polymer-Based All-Solid-State Lithium/Sulfur Battery. Advanced Functional Materials. DOI 10.1002/adfm.202104863.

[9] Chen, K. et al. (2021). An in-situ solidification strategy to block polysulfides in Lithium-Sulfur batteries. Energy Storage Materials. DOI: 10.1016/j.ensm.2021.02.012.

[10] Zhang, L. et al. (2018). The synergetic interaction between LiNO3 and lithium polysulfides for suppressing shuttle effect of lithium-sulfur batteries. Energy Storage Materials. DOI: 10.1016/j.ensm.2017.09.001.

About the sponsor: Seeing Is Solving

Evident is Empowering Solutions Through Advanced Visualization

As of April 1, 2022, Olympus Scientific Solutions Division has transitioned into a wholly owned subsidiary of Olympus and has been rebranded as Evident. Despite this change, their unwavering commitment to developing advanced solutions in the fields of life science and industry remains steadfast. Evident continues to be dedicated to creating innovative technologies that contribute to a safer and healthier world. With their extensive expertise and cutting-edge products, Evident aims to provide solutions that address the evolving needs of their customers and facilitate advancements in various industries. While Evident's name may have changed, their dedication to excellence and customer satisfaction remains the same.

Learn more about who they are.

back to content